Journal of Solid State Chemistry 182 (2009) 229–235

Contents lists available at ScienceDirect

Journal of Solid State Chemistry

journal homepage: www.elsevier.com/locate/jssc

Rare earth metal rich magnesium compounds RE_4NiMg (RE = Y, Pr–Nd, Sm, Gd–Tm, Lu)—Synthesis, structure, and hydrogenation behavior

Selcan Tuncel [a], Jean Gabriel Roquefère [b], Cristina Stan [b], Jean-Louis Bobet [b], Bernard Chevalier [b], Etienne Gaudin [b], Rolf-Dieter Hoffmann [a], Ute Ch Rodewald [a], Rainer Pöttgen [a,*]

[a] Institut für Anorganische und Analytische Chemie, Universität Münster, Corrensstrasse 30, D-48149 Münster, Germany
[b] CNRS, Université de Bordeaux, ICMCB, 87 Avenue du Docteur Albert Schweitzer, F–33608 Pessac Cedex, France

ARTICLE INFO

Article history:
Received 2 June 2008
Received in revised form
14 October 2008
Accepted 18 October 2008
Available online 5 November 2008

Keywords:
Magnesium
Intermetallics
Crystal chemistry
Hydrogenation

ABSTRACT

The rare earth metal rich compounds RE_4NiMg (RE = Y, Pr–Nd, Sm, Gd–Tm, Lu) were synthesized from the elements in sealed tantalum tubes in an induction furnace. All compounds were investigated by X-ray diffraction on powders and single crystals: Gd_4RhIn type, space group $F\bar{4}3m$, $Z = 16$, $a =$ 1367.6(2) pm for Y_4NiMg, $a = 1403.7(3)$ pm for Pr_4NiMg, $a = 1400.7(1)$ pm for Nd_4NiMg, $a = 1386.5(2)$ pm for Sm_4NiMg, $a = 1376.1(2)$ pm for Gd_4NiMg, $a = 1362.1(1)$ pm for Tb_4NiMg, $a = 1355.1(2)$ pm for Dy_4NiMg, $a = 1355.2(1)$ pm for Ho_4NiMg, $a = 1354.3(2)$ pm for Er_4NiMg, $a = 1342.9(3)$ pm for Tm_4NiMg, and $a = 1336.7(3)$ pm for Lu_4NiMg. The nickel atoms have trigonal prismatic rare earth coordination. These NiRE_6 prisms are condensed via common edges to a three-dimensional network which leaves voids for Mg_4 tetrahedra and the $RE1$ atoms which show only weak coordination to the nickel atoms. The single crystal data indicate two kinds of solid solutions. The $RE1$ positions reveal small $RE1$/Mg mixing and some compounds also show Ni/Mg mixing within the Mg_4 tetrahedra. Y_4NiMg and Gd_4NiMg have been tested for hydrogenation. These compounds absorb up to eleven hydrogen atoms per formula unit under a hydrogen pressure of 1 MPa at room temperature. The structure of the metal atoms is maintained with only an increase of the lattice parameters ($\Delta V/V \approx 22\%$) if the absorption is done at $T < 363$ K as at higher temperature a decomposition into REH_2–REH_3 hydrides occurred. Moreover, the hydrogenation affects drastically the magnetic properties of these intermetallics. For instance, Gd_4NiMg exhibits an antiferromagnetic behavior below $T_N = 92$ K whereas its hydride Gd_4NiMgH_{11} is paramagnetic down to 1.8 K.

1. Introduction

The rare earth (RE)–transition metal (T)–magnesium systems have intensively been investigated in recent years with respect to their crystal chemical peculiarities, magnetic properties and hydrogenation behavior. An overview on this topic is given in a recent review article [1]. From a structural point of view it is interesting to note, that several of the $RE_xT_yMg_z$ compounds adopt structures that are typical for indides and stannides. This is an interesting situation since reduction in the valence electron concentration through In → Mg or Sn → Mg substitution influences the magnetic behavior. To give an example, the magnetic ordering temperature of GdPdIn ($T_C = 102$ K) [2] decreases to 95.7 K in isotypic GdPdMg [3].

This indium–magnesium substitution also occurs for the recently reported structure type Gd_4RhIn [4]. Besides the indium containing series RE_4RhIn [4] and RE_4IrIn [5], also the magnesium compounds RE_4TMg (T = Co, Ru, Rh) [6–8] have been reported. We have now extended our studies of the Gd_4RhIn type intermetallics with respect to other transition elements and also for the hydrogenation behavior. Herein the different synthesis approaches for the nickel based compounds RE_4NiMg and the hydrogenation behavior of Y_4NiMg and Gd_4NiMg are reported.

2. Experimental

2.1. Synthesis

Starting materials for the preparation of the "melted" RE_4NiMg compounds were ingots of the rare earth elements (Johnson Matthey, Chempur or Kelpin), nickel wire (Johnson Matthey, ∅0.38 mm) or powder (Johnson Matthey), and a magnesium rod (Johnson Matthey, ∅16 mm); all with stated purities better than

* Corresponding author. Fax: +49 251 83 36002.
E-mail addresses: bobet@icmcb-bordeaux.cnrs.fr (J.-L. Bobet), chevalie@icmcb-bordeaux.cnrs.fr (B. Chevalier), pottgen@uni-muenster.de (R. Pöttgen).

0022-4596/$ - see front matter © 2008 Elsevier Inc. All rights reserved.
doi:10.1016/j.jssc.2008.10.026

99.9%. The surface of the magnesium rod was cut on a turning lathe in order to remove surface impurities. The rare earth metal ingots were first cut into smaller pieces and arc-melted [9] to small buttons (ca. 400 mg) under an argon atmosphere. The argon was purified with titanium sponge (900 K), silica gel, and molecular sieves.

The rare earth metal buttons, pieces of the nickel wire or nickel powder, and pieces of the magnesium rod were then weighed in the ideal 4*RE*:1Ni:1Mg atomic ratios and arc-welded in small tantalum tubes (1 cm^3 tube volume) under an argon pressure of about 80 kPa. The tantalum crucibles were then placed in a water-cooled sample chamber [10] of an induction furnace (Hüttinger Elektronik, Freiburg, Typ TIG 5/300), first heated for 2 min at about 1300 K and subsequently annealed for 2 h at ca. 920 K. Finally the crucibles were quenched to room temperature by switching off the power of the generator.

The RE_4NiMg compounds were obtained as brittle reaction products which could readily be separated from the tantalum tubes. No reaction with the container material was observed. Small single crystals were available directly from these synthesis procedures. Compact pieces and powders are stable in air for months. Powders are dark gray and single crystals exhibit metallic luster.

Alternatively, the RE_4NiMg compounds are accessible via ball-milling. This was tested for the synthesis of Y_4NiMg and Gd_4NiMg starting from the pure elemental powders of Y, Gd, Ni and Mg (purity >99.5%). The grinding procedure was carried out with a Fritsch P5 planetary ball mill. The vial (100 cm^3) loaded with 8 g of the powder and 17 stainless steel balls ($\varnothing = 10$ mm) was filled with purified argon and hermetically closed. The rotation speed of the plateau was 250 rpm and the milling time 10 h. After the milling process, the powders were pelletized manually and heated at 923 K under an argon atmosphere for 1 h to increase the crystallinity.

2.2. X-ray powder data

The RE_4NiMg samples were characterized through Guinier powder patterns using CuKα_1 radiation and α-quartz ($a = 491.30$ and $c = 540.46$ pm) as an internal standard. The Guinier camera was equipped with an imaging plate system (Fujifilm, BAS-1800). The cubic lattice parameters (Table 1) were refined by least-squares calculations. To ensure correct indexing, the experimental patterns were compared with calculated ones [11], taking the atomic positions obtained from the structure refinements.

Table 1
Lattice parameters (Guinier powder data) of the ternary magnesium compounds RE_4NiMg and the hydride Gd_4NiMgH_{11}.

Compound	a (pm)	V (nm^3)
Y_4NiMg	1367.6 (2)	2.5579
Pr_4NiMg	1403.7 (3)	2.7658
$Pr_{3.92}Ni_{1.11}Mg_{0.97}$[a]	1400.0 (2)	2.7440
Nd_4NiMg	1400.7 (1)	2.7481
$Nd_{3.94}Ni_{1.08}Mg_{0.98}$[a]	1393.8 (2)	2.7077
Sm_4NiMg	1386.5 (2)	2.6654
Gd_4NiMg	1376.1 (2)	2.6059
$Gd_{3.94}Ni_{1.08}Mg_{0.98}$[a]	1372.5 (2)	2.5855
Gd_4NiMgH_{11}	1471 (1)	3.1830
Gd_4NiMgH_{11}[a]	1468.2 (5)	3.1651
Tb_4NiMg	1362.1 (1)	2.5271
$Tb_{3.74}Ni_{1.08}Mg_{1.18}$[a]	1358.6 (2)	2.5077
Dy_4NiMg	1355.1 (2)	2.4884
Ho_4NiMg	1355.2 (1)	2.4889
Er_4NiMg	1354.3 (2)	2.4840
Tm_4NiMg	1342.9 (3)	2.4218
Lu_4NiMg	1336.7 (3)	2.3884

[a] Single crystal data.

2.3. Single crystal X-ray diffraction

Irregularly shaped crystals of RE_4NiMg (RE = Pr, Nd, Gd, Tb) were directly selected from the crushed annealed samples. Also, a crystal of the hydrogenated gadolinium sample was investigated. These crystals were glued to small quartz fibres using bees wax and first checked by Laue photographs on a Buerger camera, equipped with the same Fujifilm, BAS-1800 imaging plate technique. Intensity data were collected on a Stoe IPDS II diffractometer (graphite monochromatized MoKα radiation; oscillation mode). Numerical absorption corrections were applied to the data sets of the ternary compounds. All relevant crystallographic data for the data collections and evaluations are listed in Table 2.

2.4. Scanning electron microscopy

The single crystals investigated on the diffractometer and the bulk samples were analyzed using a Leica 420 I scanning electron microscope with the rare earth trifluorides, nickel, and magnesium oxide as standards. No impurity elements heavier than sodium (detection limit of the instrument) were observed. The compositions determined by EDX were close to the ideal one.

2.5. Hydrogenation reactions

Hydrogen sorption properties were investigated with the use of an automatic Sievert-type volumetric apparatus (HERA, Hydrogen Storage System [12]) in the temperature range between room temperature and 573 K. Before the first absorption, the sample (approximately 400 mg) was heated at 473 K under dynamic vacuum for 2 h. Then, the sample was cooled down to room temperature and the hydrogen was introduced up to 1 MPa. When no absorption occurs, the sample was heated at 373 K under vacuum for 1 h and the hydrogen is introduced again up to 1 MPa. The amount of hydrogen absorbed is deduced from the variation of the pressure in a calibrated volume (according to the Sievert method).

3. Results and discussion

3.1. Samples obtained by ball-milling

As shown in Fig. 1(a) and (c), after 10 h of ball milling, the mixed powders appeared partially amorphous. However, the major peaks relative to the RE_4NiMg phases are visible for both Y_4NiMg and Gd_4NiMg (even if it is more clear for Y_4NiMg) the same behavior has already been reported for many other compounds but especially in the case of RENi$_4$Mg which can be considered as a parent compounds as it contains the same elements but with a different stoichiometry [13]. For RENi$_4$Mg, a heat treatment at 923 K for 1 h under argon was sufficient to obtain a well crystallized product. In the case of RE_4NiMg, after annealing at 923 K for 1 h, the crystallinity remains rather low especially in the case of Gd_4NiMg (Fig. 1(b) and (d)). In order to improve the crystallinity, the effect of: (i) ball-milling and heat treatment duration and (ii) temperature of annealing should be further examined. Nevertheless, the lattice parameters determined (i.e. 1375(2) pm for Gd_4NiMg and 1368(2) pm for Y_4NiMg) are in perfect agreement with the one determined for the "melted" samples (thus elaborated in tantalum crucibles).

Table 2
Crystal data and structure refinement for RE_4NiMg and Gd_4NiMgH_{11}, Gd_4RhIn type, space group $F\bar{4}3m$, $Z = 16$; ω range 0–180°; increment 1.0°.

Empirical formula	$Pr_{3.92}Ni_{1.11}Mg_{0.97}$	$Nd_{3.94}Ni_{1.08}Mg_{0.98}$	$Gd_{3.94}Ni_{1.08}Mg_{0.98}$	Gd_4NiMgH_{11}	$Tb_{3.74}Ni_{1.08}Mg_{1.18}$
Molar mass (g/mol)	641.23	655.35	706.88	712.02	686.06
Calculated density (g/cm^3)	6.21	6.43	7.26	5.98	7.27
Crystal size (μm^3)	$10 \times 50 \times 50$	$20 \times 70 \times 80$	$20 \times 50 \times 60$	$50 \times 50 \times 50$	$20 \times 70 \times 80$
Detector distance (mm)	60	60	60	90	60
Exposure time (min)	5	5	5	13	5
Integr. param. A, B, EMS	13.0; 3.0; 0.014	13.5; 3.5; 0.012	13.0; 3.0; 0.014	13.5; 1.1; 0.039	13.5; 3.5; 0.012
Transm. ratio (max/min)	1.69	2.97	2.65	–	4.15
Absorption coefficient (mm^{-1})	30.3	32.6	42.9	35.4	44.8
$F(000)$	4385	4453	4707	4736	4598
θ range (deg)	2–35	2–35	2–35	2–31	2–35
Range in hkl	±22, ±22, ±22	±22, ±22, ±22	±21, ±21, ±21	±21, ±21, ±21	±21, ±21, ±21
Total reflections	10169	10165	9658	5094	9451
Independent reflections	631 ($R_{int} = 0.123$)	630 ($R_{int} = 0.100$)	601 ($R_{int} = 0.129$)	510 ($R_{int} = 0.123$)	591 ($R_{int} = 0.122$)
Reflections with $I > 2\sigma(I)$	457 ($R_\sigma = 0.079$)	515 ($R_\sigma = 0.051$)	490 ($R_\sigma = 0.057$)	292 ($R_\sigma = 0.072$)	496 ($R_\sigma = 0.060$)
Data/parameters	631/21	630/21	601/21	510/18	591/21
Goodness-of-fit on F^2	0.993	0.907	0.946	1.125	0.946
Final R indices [$I > 2\sigma(I)$]	$R1 = 0.036$	$R1 = 0.028$	$R1 = 0.033$	$R1 = 0.084$	$R1 = 0.027$
	$wR2 = 0.051$	$wR2 = 0.058$	$wR2 = 0.069$	$wR2 = 0.211$	$wR2 = 0.051$
R indices (all data)	$R1 = 0.054$	$R1 = 0.038$	$R1 = 0.042$	$R1 = 0.153$	$R1 = 0.035$
	$wR2 = 0.053$	$wR2 = 0.059$	$wR2 = 0.070$	$wR2 = 0.281$	$wR2 = 0.052$
Extinction coefficient	0.00019 (1)	0.00018 (2)	0.00032 (2)	–	0.00020 (2)
Flack parameter	−0.2 (2)	−0.08 (14)	−0.11 (13)	−0.1 (4)	0.00 (9)
Largest diff. peak and hole (e/Å^3)	2.13/−1.96	2.14/−1.98	2.57/−2.21	3.97/−4.66	2.67/−2.04

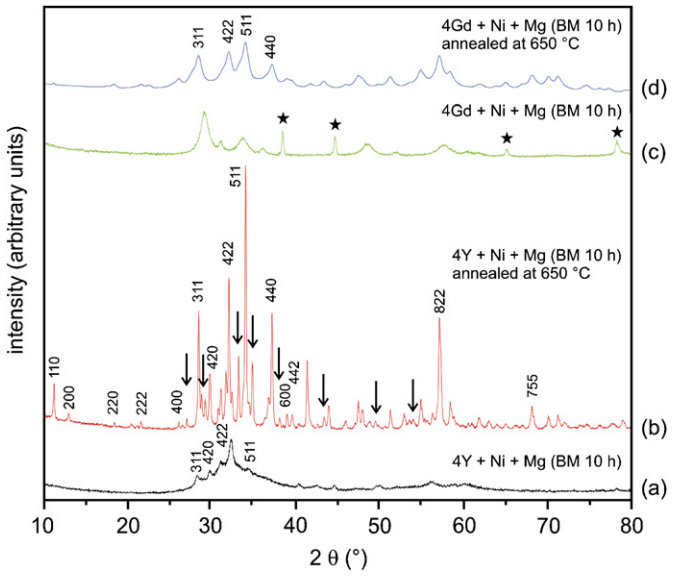

Fig. 1. X-ray diffraction patterns of Y_4NiMg and Gd_4NiMg ((a) and (c)) as milled and milled then heated at 650 °C for 1 h under Ar ((b) and (d)) (for clarity, all the first peaks up to 442 are marked and then only the more intense ones; the unindexed impurity peaks are highlighted with an arrow and the stars indicated the peaks relative to the aluminum sample holder).

However, it is also worth pointing out that some peaks cannot be indexed on the XRD patterns and are due to some impurities induced by the ball milling process. As a partial conclusion, the ball-milling appears as a method to synthesize RE_4NiMg compounds but the obtained product is not single phase. For that reason, H sorption and magnetic measurements have not been performed on these products but only on the 'melted' ones.

3.2. Structure refinements

The IDPS data sets of all crystals showed face-centered cubic cells and no further systematic extinctions in agreement with our previous investigations on the RE_4TMg compounds (T = Co, Ru, Rh) [6–8]. Space group $F\bar{4}3m$ was found to be correct during the structure refinements. The atomic parameters of La_4CoMg [6] were taken as starting values and the structures were refined with anisotropic displacement parameters for all atoms with SHELXL-97 (full-matrix least-squares on F_0^2) [14]. Refinement of the correct absolute structure was ensured through calculation of the Flack parameters [15,16]. Since most RE_4TMg compounds revealed some mixed occupied sites, the occupancy parameters were refined in separate series of least-squares cycles. Also for the nickel based series RE_1/Mg and Mg/Ni mixing were observed. These mixed occupancies were refined as least-squares variables in the final cycles, leading to the compositions listed in Table 3. Final difference Fourier syntheses revealed no significant residual peaks. The refinements then converged to the residuals listed in Table 2 and the atomic parameters and interatomic distances listed in Tables 3 and 4 (exemplarily for Gd_4NiMg and the hydride). Further data on the structure refinements are available.[1]

The crystal of the hydrogenated sample based on gadolinium revealed the highest residuals. It is always difficult to extract high quality single crystals from such hydrogenated samples, since hydrogen insertion leads to a decrease of the crystallinity. Similar to the other RE_4TMg phases [4–8], also this crystal was twinned, and only the non-overlapping reflections of one domain were used for the structure refinement. At the present stage, the refined metal sites can only be considered as the average structure. The enlarged displacement parameters account for the most likely occurring symmetry reduction. However, in the absence of precise neutron powder diffraction data and the low crystal quality, more detailed structural information can definitely not be extracted.

3.3. Crystal chemistry

New intermetallic magnesium compounds RE_4NiMg (RE = Y, Pr–Nd, Sm, Gd–Tm, Lu) have been synthesized and structurally characterized. They crystallize with the non-centrosymmetric Gd_4RhIn type structure, space group $F\bar{4}3m$. The cell volume

[1] Details may be obtained from: Fachinformationszentrum Karlsruhe, D-76344 Eggenstein-Leopoldshafen (Germany), by quoting the Registry Nos'. CSD–419526 ($Pr_{3.92}Ni_{1.11}Mg_{0.97}$), CSD–419527 ($Nd_{3.94}Ni_{1.08}Mg_{0.98}$), CSD–419528 ($Gd_{3.94}Ni_{1.08}Mg_{0.98}$), CSD–419525 ($Gd_4NiMgH_{11}$), and CSD–419529 ($Tb_{3.74}Ni_{1.08}Mg_{1.18}$).

Table 3
Atomic coordinates and isotropic displacement parameters (pm^2) of *some* RE_4NiMg compounds and the hydride Gd_4NiMgH_{11}.

Atom	Wyckoff site	*x*	*y*	*z*	U_{eq}
$Pr_{3.92}Ni_{1.11}Mg_{0.97}$					
94.7(9)% Pr1/5.3(9)% Mg2	24*g*	0.43558 (9)	3/4	3/4	134 (4)
Pr2	24*f*	0.81053 (9)	0	0	126 (3)
Pr3	16*e*	0.65383 (7)	x	x	116 (3)
Ni1	16*e*	0.85801 (14)	x	x	156 (7)
89(3)% Mg1/11(3)% Ni2	16*e*	0.4208 (3)	x	x	164 (27)
$Nd_{3.94}Ni_{1.08}Mg_{0.98}$					
96.0(7)% Nd1/4.0(7)% Mg2	24*g*	0.43559 (5)	3/4	3/4	137 (3)
Nd2	24*f*	0.81072 (6)	0	0	130 (2)
Nd3	16*e*	0.65387 (4)	x	x	119 (2)
Ni1	16*e*	0.85826 (10)	x	x	162 (5)
92(2)%Mg1/8(2)%Ni2	16*e*	0.4206 (2)	x	x	161 (19)
$Gd_{3.94}Ni_{1.08}Mg_{0.98}$					
95.9(9)% Gd1/4.1(9)% Mg2	24*g*	0.56519 (7)	1/4	1/4	139 (3)
Gd2	24*f*	0.18818 (7)	0	0	129 (2)
Gd3	16*e*	0.34627 (5)	x	x	125 (2)
Ni1	16*e*	0.14178 (14)	x	x	167 (6)
92(3)% Mg1/8(3)% Ni2	16*e*	0.5797 (3)	x	x	196 (27)
Gd_4NiMgH_{11}					
Gd1	24*g*	0.4348 (3)	3/4	3/4	927 (22)
Gd2	24*f*	0.8061 (4)	0	0	782 (15)
Gd3	16*e*	0.6519 (2)	x	x	553 (12)
Ni1	16*e*	0.8594 (6)	x	x	790 (41)
Mg	16*e*	0.419 (1)	x	x	577 (70)
$Tb_{3.74}Ni_{1.08}Mg_{1.18}$					
82.4(6)% Tb1/17.6(6)% Mg2	24*g*	0.56606 (6)	1/4	1/4	136 (3)
Tb2	24*f*	0.18870 (6)	0	0	124 (2)
Tb3	16*e*	0.34645 (4)	x	x	114 (2)
Ni1	16*e*	0.14151 (11)	x	x	151 (5)
92(2)% Mg1/8(2)% Ni2	16*e*	0.5807 (3)	x	x	204 (23)

U_{eq} is defined as one third of the trace of the orthogonalized U_{ij} tensor.

Table 4
Interatomic distances (pm), calculated with the powder lattice parameters of $Gd_{3.94}Ni_{1.08}Mg_{0.98}$ and the single crystal data of Gd_4NiMgH_{11}.

	$Gd_{3.94}Ni_{1.08}Mg_{0.98}$	Gd_4NiMgH_{11}	
Gd1:			
2	Mg	331.2 (6)	352 (2)
2	Ni	353.3 (1)	378.0 (4)
2	Gd3	353.8 (1)	378.3 (4)
4	Gd1	358.7 (1)	383.7 (7)
4	Gd2	364.6 (1)	388.2 (2)
Gd2:			
2	Ni	282.5 (2)	302.2 (10)
2	Mg	354.2 (2)	370.9 (7)
4	Gd1	364.6 (1)	388.2 (2)
4	Gd2	365.3 (1)	402.7 (7)
2	Gd3	368.9 (1)	388.3 (3)
Gd3:			
3	Ni	281.6 (2)	305.6 (10)
3	Mg	351.1 (2)	372.3 (8)
3	Gd1	353.8 (1)	378.3 (4)
3	Gd2	368.9 (1)	388.3 (3)
3	Gd3	373.7 (2)	407.2 (9)
Ni:			
3	Gd3	281.6 (2)	305.6 (10)
3	Gd2	282.5 (2)	302.2 (10)
3	Gd1	353.3 (1)	378.0 (4)
Mg:			
3	Mg	309 (1)	336 (5)
3	Gd1	331.2 (6)	352 (2)
3	Gd3	351.1 (2)	372.3 (8)
3	Gd2	354.2 (2)	370.8 (7)

Standard deviations are given in parentheses. All distances within the first coordination spheres are listed. Note that the Gd1 and Mg positions in $Gd_{3.94}Ni_{1.08}Mg_{0.98}$ reveal mixed occupancies (see Table 3).

(Table 1) decreases from the lanthanum to the lutetium compound as expected from the lanthanoid contraction. Y_4NiMg has a cell volume close to Gd_4NiMg, similar to the other RE_4TMg series [6–8].

The striking structural motifs are nickel centered trigonal prisms RE_6 formed by the rare earth atoms *RE*2 and *RE*3 with relatively short *RE*–Ni distances. As an example the Gd_4NiMg structure is discussed here. The Gd2–Ni and Gd3–Ni distances of 282 and 283 pm are close to the sum of the covalent radii [17] of 276 pm. indicating strong bonding between *RE* and Ni. Similar short Gd–Ni distances occur in the two-dimensional network of condensed trigonal prisms of $Gd_{14}Ni_{3.29}In_{2.71}$ [18]. In Gd_4NiMg the trigonal prisms Gd_6 are condensed via common edges (Fig. 2). This rigid network leaves larger voids that are filled with the Mg_4 tetrahedra and the *RE*1 atoms. Similar to the ruthenium based compounds [8], some Ni/Mg mixing on the Mg_4 tetrahedra is also observed. For further crystal chemical details we refer to our previous works on isotypic indides and magnesium compounds RE_4TIn [4,5] and RE_4TMg [6–8].

Finally we comment on the crystallographic data of a crystal from the hydrogenated gadolinium compound Gd_4NiMgH_{11}. The lattice parameter of the hydride was larger than the one taken from the ternary sample (Table 1) as expected after hydrogen absorption. No major difference between the atomic sites of the intermetallic and the hydrogenated sample can be found (Table 3). We observe more or less an isotropic expansion of the structure.

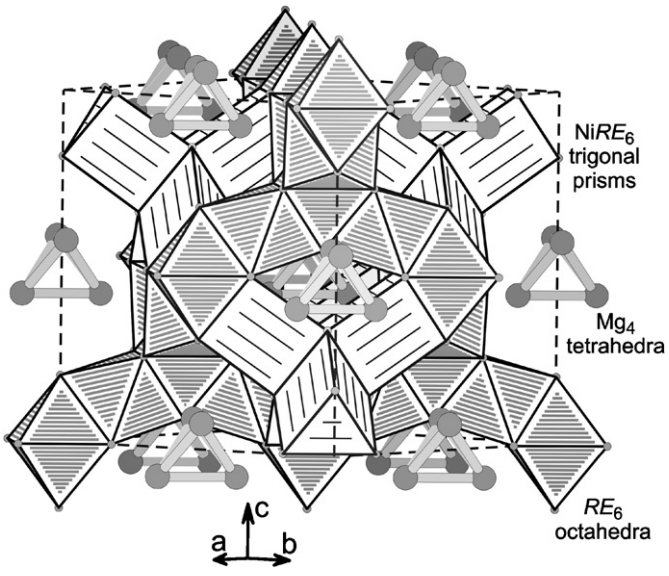

Fig. 2. View of the RE_4NiMg structure approximately along the [110] direction. The Mg_4 tetrahedra, the network of condensed NiRE_6 trigonal prisms and the empty RE_6 octahedra are emphasized. For details see text.

From the X-ray data we can only postulate potential hydrogen sites. These can be the empty octahedra shown in Fig. 2, but also the tetrahedral sites left by condensation of three trigonal prisms.

Deuteration experiments on samples of Y_4NiMg and Tb_4NiMg are in progress in order to study the structure by neutron diffraction.

In Fig. 3 we present a comparison of the two central structural motifs in the structures of Gd_4NiMg and Gd_4NiMgH_{11}, i.e. the Mg_4 tetrahedra and the $NiGd_6$ trigonal prisms. The structure of the hydride reveals two distinct features: (i) overall large isotropic displacement parameters (Table 3) and (ii) a drastic increase of the interatomic distances (Table 4). The cubic structure model of Gd_4NiMgH_{11} presented herein can certainly only be considered as average structure. The hydrogen insertion induces distortions and the enlarged displacement parameters account for the different sites. Similar to the many other transition metal-based hydrides, the nickel atoms in the hydrogenated phase Gd_4NiMgH_{11} most likely also show Ni–H coordination, as recently observed in the structures of $LaNiMg_2H_7$ [19] and $La_2Ni_2MgH_8$ [20]. Ongoing neutron and high-resolution synchrotron diffraction studies on deuterated samples of Y_4NiMg and Tb_4NiMg will shed more light on the structural behavior of these hydrides.

3.4. Hydrogenation behavior

Both Gd_4NiMg and Y_4NiMg have been subjected to hydrogen pressure from room temperature to 523 K. The absorption starts, respectively, around 313 and 323 K. As seen in Fig. 4 (only the Gd_4NiMg kinetics is presented to clarify the graph), a latency period exists prior any absorption and is slightly influenced by the temperature. It is worth pointing out that a new and fresh sample was used for each new absorption experiment. The absorption is rather fast as the full sorption capacity is always reached in less than 10 min. The sorption kinetics increase with increasing temperature. The maximum hydrogen uptake is almost independent of the temperature and is 1.58 and 2.32 wt% for Gd_4NiMg and Y_4NiMg, respectively, which corresponds to 11.3 and 10.2 hydrogen atoms per formula unit (H/f.u.). Such values close to 2H/*M* (*M* = number of atoms by f.u.) is considered as very high compared with the sorption capacity of other well known intermetallics (e.g. approximately 1.2H/*M* for AB_5 and 1.33H/*M* for AB_2 compounds [21]) but it is in fact close to the values generally observed for *A* metals like Mg, Ti, or *RE*.

However, no desorption has been observed under vacuum up to 373 K. On Fig. 5 are presented the XRD patterns obtained after absorption at various temperatures in the case of Gd_4NiMg. A very interesting behavior can be highlighted: with an increase of the temperature the crystallinity decreases drastically. The estimated crystallites size (by the Warren Averbach method) decreases from 40 nm in the initial intermetallic to 10 nm for the hydride prepared at 363 K (and 25 nm for the one prepared at 323 K). The low crystallinity seems to indicate that as already observed for the cubic Laves phase AB_2 an hydrogen induced amorphization [22] is occurring in our compounds Therefore, it should also be noticed that at higher temperature (i.e. more than 363 K) the intermetallic decomposed under hydrogen and the formation of GdH_2/GdH_3 (with very low crystallinity) is observed. We assumed that at temperature higher than 363 K, the formation of REH_2/REH_3 is thermodynamically favored so that the initial compounds decomposed. Nevertheless, it is not possible from this stage whether the disproportionation and amorphization of the metallic hydride or the amorphization of the hydride and its subsequent disproportionation is coming first. Therefore, under vacuum at 573 K, the desorption is observed but from MgH_2 and GdH_3 (i.e. no reversible desorption).

The lattice parameter of the hydrided phase is 1471 pm (powder data) which corresponds to an increase of the molar cell volume of 22.1%. Such a high increase of the volume is in good agreement with the high amount of hydrogen uptake and explains also the decrease of the crystallinity during the sorption. The XRD patterns presented in Fig. 5 also reveal the presence of some impurities in the initial compounds. The EPMA highlights the presence of Gd_3Ni and the unindexed peaks are perfectly fitting with the structure of Gd_3Ni.

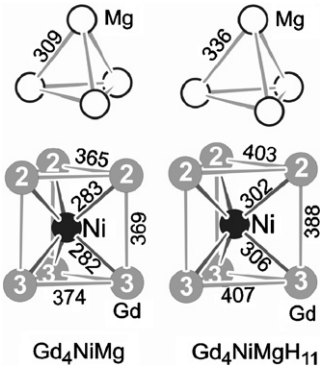

Fig. 3. The Mg_4 and $NiGd_6$ units in the structures of Gd_4NiMg and Gd_4NiMgH_{11}. Relevant interatomic distances are indicated.

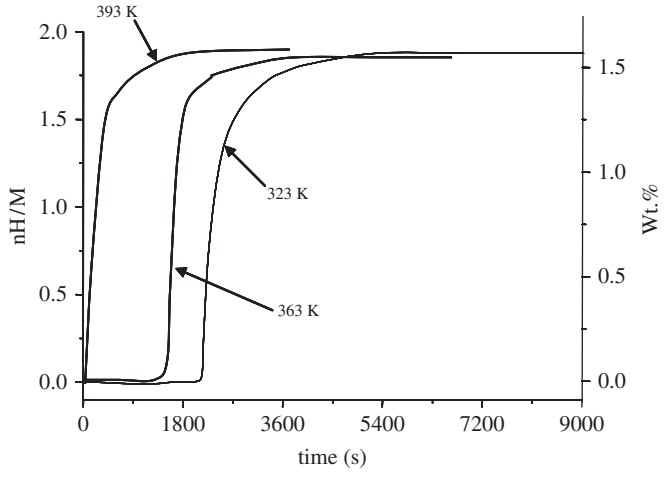

Fig. 4. Time dependence of the hydrogen absorption of Gd_4NiMg at various temperature and under a constant pressure of 1 MPa.

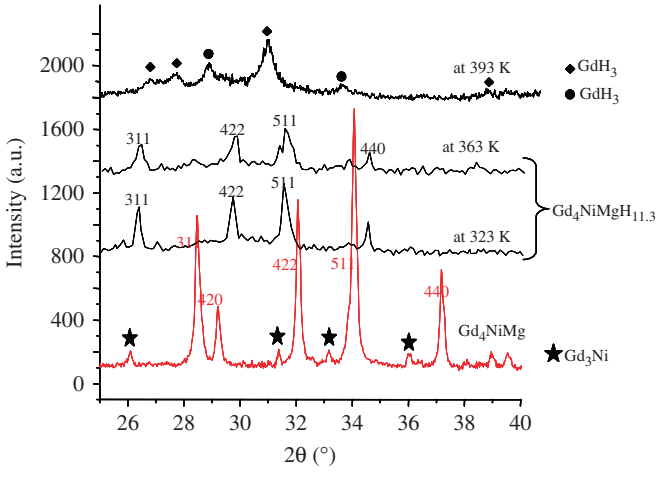

Fig. 5. XRD patterns for Gd_4NiMg before and after hydrogenation at various temperatures (at 323 and 363 K, formation of $Gd_4NiMgH_{11.3}$ and at 393 K, decomposition and formation of GdH_2/GdH_3). The impurity Gd_3Ni present in the initial sample is identified with stars on the pattern.

3.5. Magnetic properties

The temperature dependence of the magnetic susceptibility χ_m of Gd_4NiMg, measured in an applied magnetic field of 0.1 T, exhibits a maximum at $T_N = 92$ K (Fig. 6). This behavior characterizes the occurrence of antiferromagnetic ordering. The Néel temperature T_N of Gd_4NiMg is comparable to that determined for the binary intermetallic Gd_3Ni ($T_N = 100$ K) that contains also a higher gadolinium atomic concentration [23]. Above 175 K, the reciprocal magnetic susceptibility χ_m^{-1} of Gd_4NiMg, measured with an applied field of 3 T (Fig. 7), follows a Curie–Weiss law $\chi_m^{-1} = (T - \theta_p)/C_m$ where θ_p is the paramagnetic Curie temperature and C_m the Curie constant per formula unit. The experimental value of the effective magnetic moment $\mu_{eff} = (8C_m)^{1/2} = 8.24\,\mu_B$/Gd is higher than that calculated one for a free Gd^{3+}-ion (7.94 μ_B/Gd).

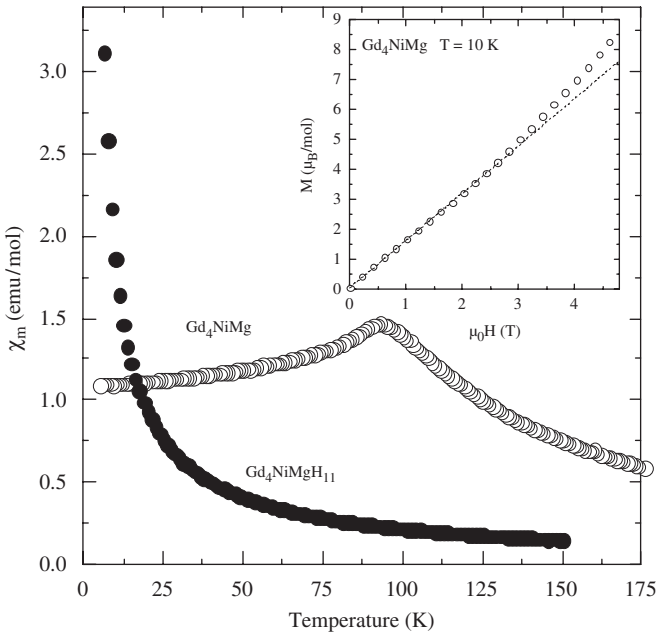

Fig. 6. Temperature dependence of the magnetic susceptibility of Gd_4NiMg and its hydride measured with an applied magnetic field of 0.1 T. The inset presents the field dependence of the magnetization of Gd_4NiMg at 10 K.

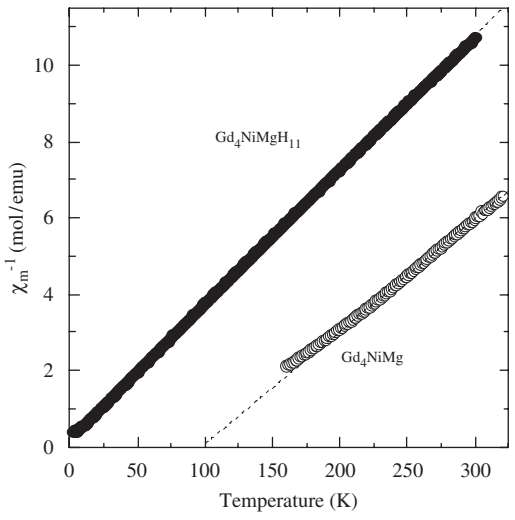

Fig. 7. Temperature dependence of the reciprocal magnetic susceptibility of Gd_4NiMg and its hydride. The dashed lines present the Curie–Weiss law (see text).

This μ_{eff}-value suggests: (i) that the nickel atoms might carry a magnetic moment in this ternary compound as reported for $GdNi_2$ [24] or (ii) that the conduction electrons contribute to the magnetic properties of this intermetallic as observed for the gadolinium metal [25]. The paramagnetic Curie temperature θ_p of Gd_4NiMg is found positive and equals to 97 K. The existence of the maximum on the $\chi_m = f(T)$ curve (Fig. 6) at T_N and the positive value of θ_p are rather unusual for classical antiferromagnets. These data give some support that in Gd_4NiMg both positive and negative exchange interactions exist perhaps linked to the presence of three different atomic positions for gadolinium in the crystal structure of this compound. Similar behavior was reported for the antiferromagnet Gd_3Ni ($T_N = 100$ K) which shows also a positive paramagnetic Curie temperature of $\theta_p = 87$ K. In this way, it is interesting to note that Gd_4NiMg exhibits below $T_N = 92$ K a metamagnetic transition; for instance, at 10 K, its magnetization increases linearly at low fields and more rapidly around 2.5–3 T (inset of Fig. 6).

On the contrary, no magnetic ordering can be detected above 1.8 K by magnetic susceptibility measurements performed on the hydride deriving from Gd_4NiMg (Fig. 7); its χ_m susceptibility increases monotonically with decreasing temperature without any indication of ordering. Above 6 K, the $\chi_m^{-1} = f(T)$ curve follows a Curie–Weiss law (Fig. 7) with $\mu_{eff} = 7.55\,\mu_B$/Gd as effective moment and a small negative $\theta_p = -7$ K temperature. In other words, the hydrogenation of Gd_4NiMg destroys its antiferromagnetic ordering. The hydrogen insertion induces a significant increase of the Gd–Gd interatomic distances (Table 4) and then leads to weakening of the Gd–Gd magnetic interactions in agreement with the small value of θ_p [3]. The Gd–Gd distances play an important role on the indirect RKKY-magnetic interaction responsible of the magnetic properties of the compounds based on rare earth. In many cases, the hydrogen insertion induces a decrease of the magnetic ordering; for instance the Curie temperature decreases from 118 to 69 K during the hydrogenation of $Gd_3Ni_6Al_2$ [26].

4. Conclusion

The rare earth metal rich compounds RE_4NiMg (RE = Y, Pr–Nd, Sm, Gd–Tm, Lu) crystallize with the Gd_4RhIn structure type. The centered trigonal prisms of RE (i.e. $NiRE_6$) are condensed via common edges to build a three-dimensional network which ensures the rigidity of the structure. The relative large number of voids in the structure enables hydrogen absorption at room temperature and moderate pressure (i.e. 1 MPa). The compounds absorb approximately 11H per formula unit and no structural change was observed, except a large increase of the unit cell volume ($\Delta V/V \approx 22\%$). Therefore, it is also noticed that at temperatures higher than 363 K, the hydride decomposed into REH_2/REH_3 and elemental metals. Finally, it is also reported that hydrogen absorption induces a drastic change of the magnetic properties of Gd_4NiMg as the intermetallic exhibits an antiferromagnetic behavior below 92 K whereas the hydride is paramagnetic down to 1.8 K.

Acknowledgments

We thank Dipl.-Chem. F.M. Schappacher for the work at the scanning electron microscope. This work was financially supported by the Deutsche Forschungsgemeinschaft. B.C., E.G. and R.P. are indebted to EGIDE and DAAD for research grants within the Procope programs (11457RD and D/0502176).

References

[1] U.Ch. Rodewald, B. Chevalier, R. Pöttgen, J. Solid State Chem. 180 (2007) 1720.
[2] J.W.C. de Vries, R.C. Thiel, K.H.J. Buschow, J. Less-Common Metals 111 (1985) 313.
[3] K. Łątka, T. Tomkowicz, R. Kmieć, A.W. Pacyna, R. Mishra, T. Fickenscher, R.-D. Hoffmann, R. Pöttgen, H. Piotrowski, J. Solid State Chem. 168 (2002) 331.
[4] R. Zaremba, U.Ch. Rodewald, R.-D. Hoffmann, R. Pöttgen, Monatsh. Chem. 138 (2007) 523.
[5] R. Zaremba, U.Ch. Rodewald, R.-D. Hoffmann, R. Pöttgen, Monatsh. Chem. 139 (2008) 481.
[6] S. Tuncel, R.-D. Hoffmann, B. Chevalier, S.F. Matar, R. Pöttgen, Z. Anorg. Allg. Chem. 633 (2007) 151.
[7] S. Tuncel, U.Ch. Rodewald, B. Chevalier, R. Pöttgen, Z. Naturforsch. 62b (2007) 642.
[8] S. Tuncel, B. Chevalier, S.F. Matar, R. Pöttgen, Z. Anorg. Allg. Chem. 633 (2007) 2019.
[9] R. Pöttgen, Th. Gulden, A. Simon, GIT Labor Fachz. 43 (1999) 133.
[10] D. Kußmann, R.-D. Hoffmann, R. Pöttgen, Z. Anorg. Allg. Chem. 624 (1998) 1727.
[11] K. Yvon, W. Jeitschko, E. Parthé, J. Appl. Crystallogr. 10 (1977) 73.
[12] R. Schulz, S. Boily, J. Huot, J. Canadian Patent, Ser. No. 2207149, 1999.
[13] J.-L. Bobet, P. Lesportes, J.-G. Roquefère, B. Chevalier, K. Asano, K. Sakaki, E. Akiba, Int. J. Hydrogen Energy 32 (2007) 2422.
[14] G.M. Sheldrick, SHELXL-97, Program for Crystal Structure Refinement, University of Göttingen, Germany, 1997.
[15] H.D. Flack, G. Bernadinelli, Acta Crystallogr. A 55 (1999) 908.
[16] H.D. Flack, G. Bernadinelli, J. Appl. Crystallogr. 33 (2000) 1143.
[17] J. Emsley, The Elements, Oxford University Press, Oxford, 1999.
[18] M. Lukachuk, Ya.V. Galadzhun, R.I. Zaremba, M.V. Dzevenko, Ya.M. Kalychak, V.I. Zaremba, U.Ch. Rodewald, R. Pöttgen, J. Solid State Chem. 178 (2005) 2724.
[19] G. Renaudin, L. Guénée, K. Yvon, J. Alloys Compd. 350 (2003) 145.
[20] J.-N. Chotard, Ya. Filinchuk, B. Revaz, K. Yvon, Angew. Chem. Int. Ed. 45 (2006) 7770.
[21] L. Schlapbach, A. Züttel, Nature 414 (2001) 353.
[22] K. Aoki, T. Masumoto, J. Alloys Compd. 194 (1993) 251.
[23] E. Talik, Physica B 193 (1994) 213.
[24] K. Yano, I. Umehara, T. Miyazawa, Y. Adachi, K. Sato, Physica B 367 (2005) 81.
[25] M. Colarieti-Tosti, S.I. Simak, R. Ahuja, L. Nordström, O. Eriksson, D. Aberg, S. Edvardsson, M.S.S. Brooks, Phys. Rev. Lett. 91 (2003) 157201.
[26] S. Pechev, B. Chevalier, M. Khrussanova, M. Terzieva, J.-L. Bobet, B. Darriet, P. Peshev, J. Alloys Compd. 259 (1997) 24.